Nature of visons in the perturbed ferromagnetic and antiferromagnetic Kitaev honeycomb models

Chuan Chen [1,*] and Inti Sodemann Villadiego [2,3,†]

[1]*Institute for Advanced Study, Tsinghua University, 100084 Beijing, China*
[2]*Institut für Theoretische Physik, Universität Leipzig, 04103 Leipzig, Germany*
[3]*Max-Planck Institute for the Physics of Complex Systems, 01187 Dresden, Germany*

The Kitaev honeycomb model hosts a fascinating fractionalized state of matter featuring emergent Majorana fermions and a vison particle that carries the flux of an emergent gauge field. In the exactly solvable model these visons are static, but certain perturbations can induce their motion. We show that the nature of the vison motion induced by a Zeeman field is sharply distinct in the ferromagnetic vs the antiferromagnetic Kitaev models. Namely, in the ferromagnetic model the vison has a trivial nonprojective translational symmetry, whereas in the antiferromagnetic Kitaev model it has a projective translational symmetry with π flux per unit cell. The vison band of the ferromagnetic case has zero Berry curvature and no associated intrinsic contribution to the thermal Hall effect. In contrast, in the antiferromagnetic case there are two gapped vison bands with opposite Chern numbers and an associated intrinsic vison contribution to the thermal Hall effect. We discuss these findings in light of the physics of the spin liquid candidate α-RuCl$_3$.

I. INTRODUCTION

The Kitaev honeycomb model [1] has become a paradigmatic playground to investigate spin liquids with emergent fermions and Z_2 gauge fields in two dimensions. Unlike other exactly solvable models, the model only contains spin bilinear interactions, and it is believed to be a reasonable description of certain quantum magnets, such as α-RuCl$_3$ [2–4]. Although α-RuCl$_3$ forms a zigzag antiferromagnet in the absence of applied magnetic fields [5–7], there are several experimental indications that it might harbor a quantum spin liquid once an in-plane magnetic field is applied within the range of $\sim$6–11 T [8–18].

Nevertheless, the connection between the experimentally observed potential spin liquid in α-RuCl$_3$ and the spin liquids realized in the weakly perturbed ideal Kitaev model is currently far from clear. This stems in part from the lingering uncertainty regarding the minimal Heisenberg-type model describing the material. The largest coupling term in α-RuCl$_3$, denoted by K, is in fact believed to be the term that appears in the ideal Kitaev model. While a majority of studies have advocated that this coupling is ferromagnetic (FM, $K < 0$), others have advocated for an antiferromagnetic (AFM, $K > 0$) exchange coupling (see Refs. [19,20] for tables summarizing the estimates of several studies). Some of the prominent observational evidence favoring K to be ferromagnetic comes from elastic x-ray scattering experiments [21] that determined the direction of the ordered moment in the zigzag AFM state, which is dependent on the sign of K [22]. Inelastic x-ray scattering experiments [23] have also advocated for a fer-

romagnetic coupling. However, these experiments relied on modeling the zigzag AFM state, which is highly susceptible to perturbations and itself subjected to very strong quantum fluctuations. Therefore we believe that there is still some room to be reasonably skeptical about the certainty of the sign of this coupling. Determining this sign is crucial for many reasons. For example, the spin liquid realized in the AFM coupled case is more robust to certain perturbations, as compared with the spin liquid realized for the FM coupled case [24–27]. Additionally, the nature of the phases driven by the applied Zeeman field can be very different in both cases, displaying a delicate dependence on the further-neighbor exchange couplings allowed by symmetry, such as the Γ, Γ', J, and J_3 terms [3,19,20,24–30].

In this paper we will further emphasize the importance of the sign of K by demonstrating that the FM Kitaev model is in a sharply distinct topological phase compared with the AFM Kitaev model in the presence of a Zeeman field. More specifically, we will show that even though the FM and AFM Kitaev models realize ground states within the same celebrated Ising topological order, they realize distinct symmetry-enriched topological orders with regard to the translational symmetry of the lattice and therefore belong to two distinct universality classes. This distinction manifests vividly in the properties of their vison quasiparticles [31–34], the vison being the emergent non-Abelian anyon analogous to a π flux in a $p + ip$ superconductor that carries a Majorana fermion zero mode in its core [35].

We will show that for the FM Kitaev model, lattice translations act on the vison in an ordinary nonprojective way. This implies that the vison Bravais lattice contains a single state per unit cell associated with each hexagon of the honeycomb lattice [see Fig. 1(a)], and as a consequence its Berry curvature vanishes everywhere in its Brillouin zone. One important

*chuanchen@tsinghua.edu.cn
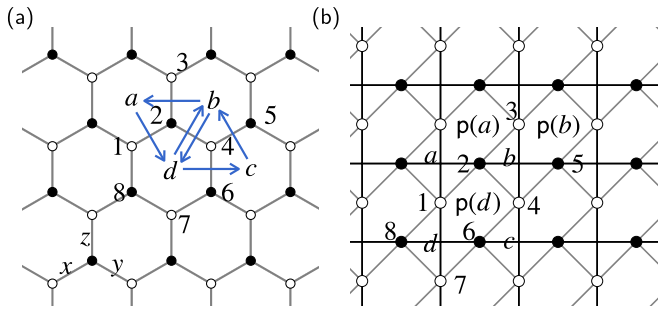†sodemann@itp.uni-leipzig.de

FIG. 1. (a) Honeycomb lattice of the Kitaev model. The x, y, and z links are labeled. The visons are located at the center of the hexagons, e.g., a, b, c, and d highlighted in the schematic. A- and B-sublattice sites are represented by open and solid circles, respectively. (b) The tilted honeycomb lattice with vertices placed on the links of a square lattice. Visons are now located at the vertices of the square lattice, while the ε fermions sit at plaquettes. A-sublattice sites of the original honeycomb lattice now all align on vertical links of the square lattice.

aspect that we will emphasize in this paper is that in order to correctly capture the motion of the vison induced by the Zeeman field, it is crucial to include the Haldane mass term that is generated perturbatively by the Zeeman field on the itinerant Majorana fermions. Such a term is strictly necessary in order to make the state a fully gapped topologically ordered phase of matter and to make the vison an exponentially localized particle. In fact, we will directly show numerically that in finite-size systems the phase that the vison acquires is highly sensitive to system size and boundary conditions when the Haldane mass of the Majorana is set to be exactly zero. On the other hand, we will also show numerically that as the thermodynamic limit is approached any small but nonzero Haldane mass term is sufficient in order to regularize and obtain a unique and well-defined phase for the visons as they move around a unit cell of the Bravais lattice.

On the other hand, we will show that for the AFM Kitaev model the presence of the Haldane mass term leads to a finite vison hopping. We will show that interestingly, in the AFM case, the vison has indeed projective translations with π flux per unit cell allowing it to have a finite Berry curvature and two Chern bands with Chern numbers $C = \pm 1$. We will also show, in agreement with Ref. [36], that perturbatively in the applied Zeeman field, the vison in the FM Kitaev model has a larger bandwidth than in the AFM Kitaev model, so the vison band minimum reaches zero faster in the former (FM) case as the Zeeman field increases (see Fig. 5 for a plot of vison bands in both FM and AFM Kitaev models). This is crucially related to the stability of the latter against Zeeman perturbations that would stabilize competing ordered phases, because some of these instabilities could be viewed as gauge confinement transitions driven by vison condensation that would appear as its bandwidth increases and the vison gap closes at certain momenta.

Our work is also interesting from the point of view of the mathematical methods that we exploit to compute these properties. In fact, our results are an application of an exact lattice operator duality recently developed in Ref. [37], which extended the mapping of Ref. [38], from the underlying local

spin degrees of freedom onto nonlocal fermion (spinon) and hard-core boson (vison) degrees of freedom. For related ideas and developments, see also Refs. [39–41]. Our methods could also be useful for investigating other experimentally relevant observables, such as the static and dynamic spin correlation functions [42–46].

This paper is organized as follows: In Sec. II, we introduce and review the model of interest, which is the Kitaev model perturbed by a Zeeman field. We then discuss how the Zeeman couplings could induce vison hoppings in Sec. III A, and we set up the general formulas that define the vison hopping amplitudes and the phases associated with vison hopping around small closed loops of the lattice. In Sec. III B, we review the recently developed exact duality mapping [37] and discuss how to explicitly compute the vison hopping amplitudes and phases defined in Sec. III A. Section IV contains the main results of this study. Section IV A presents the explicit numerical results of the vison hopping amplitudes and phases for both FM and AFM coupled models. In Sec. IV B we show that for the AFM case the vison bands are topologically nontrivial and carry a finite Berry curvature and nonzero Chern numbers. In Sec. V we provide additional evidence for our conclusions, by showing that the vison phases around loops agree with those of certain commuting projector Hamiltonians where calculations can be performed fully analytically. Finally, in Sec. VI, we summarize our findings and make some suggestions for guiding experimental efforts to further determine the sign of K in α-RuCl$_3$. Appendix A discusses the dependence on boundary conditions for both FM and AFM models, and Appendix B discusses details of finite-size effects and the infinite-size extrapolation of our results.

II. KITAEV MODEL PERTURBED BY A ZEEMAN FIELD

The model of interest is the Kitaev honeycomb model with a Haldane mass term [1]:

$$H = H_K - \kappa \sum_{i,j,k} X_i Y_j Z_k,$$

$$H_K = K \left(\sum_{x \text{ links}} X_i X_j + \sum_{y \text{ links}} Y_i Y_j + \sum_{z \text{ links}} Z_i Z_j \right). \quad (1)$$

Here, X_i, Y_j, and Z_k are the Pauli matrices of spins residing in the sites of the honeycomb lattice [see Fig. 1(a)]. The above Hamiltonian is exactly solvable and features a dispersive band of itinerant Majorana fermions and a gapped flat band of visons with an energy $E_0 \approx 0.15|K|$ for $|\kappa| \ll |K|$ [1]. The term κ induces a Haldane mass on the Majorana fermions that would otherwise have a gapless dispersion (see Ref. [1] for the choice of i, j, k in the summation). Therefore this term is needed in order to have a fully gapped topologically ordered state and exponentially localized Majorana zero modes carried by the vison. Throughout this paper we will keep κ as an *independent* parameter of the model, but we will view it implicitly as a term that is perturbatively generated by a physical Zeeman field, whose leading form is $\kappa \approx h_x h_y h_z / K^2$ [1]; in particular, in all of our subsequent discussions it is understood that we fix $\text{sgn}(\kappa) = \text{sgn}(h_x h_z h_y)$. It should be noted that in the presence of other types of perturbations, the

induced Haldane mass term can scale linearly with h [46]; therefore a finite κ term is physically relevant in those cases as well.

In addition to the above, we include the following explicit Zeeman coupling to H in Eq. (1):

$$\Delta H = -\sum_j (h_x X_j + h_y Y_j + h_z Z_j). \quad (2)$$

The above term is produced by an external magnetic field. Crucially, this term induces not only the aforementioned Haldane mass term (provided that each component of the magnetic field is nonzero), but also the motion and pair creation or annihilation of the vison particles, destroying the exact solvability of the model. We will therefore treat this term as a perturbation. Our goal is to compute the perturbative hoppings and band dispersions that this term induces on the visons and to compute the real-space phases that result from such vison motion when it is transported around a unit cell of its triangular lattice. While the magnitude of these hoppings will depend on the detailed form of the perturbation that induces the vison hopping, we wish to emphasize that this phase is independent of the specific detailed form of the operator that induces the vison motion, as long as it respects translational symmetry, since this phase is a universal property of the topologically ordered state enriched by translational symmetry, as recently argued in Ref. [37]. Therefore, as we will see, this phase is in exact agreement with the phase that was computed in Ref. [37] with a perturbation different from the Zeeman field.

III. METHODS

A. Vison hoppings in the honeycomb lattice

The visons can be viewed as being located at the center of each hexagon. The vison parity operator at a hexagon or plaquette p, W_p, equals -1 (1) when a vison is present (absent) in a plaquette, and it is a product of the Pauli matrices of the six spins surrounding p [1]. For example, for the hexagon d in Fig. 1(a), we have

$$W_d = X_4 Y_6 Z_7 X_8 Y_1 Z_2. \quad (3)$$

For H in Eq. (1), the vison parity W_p is a constant of motion. However, its value (± 1) can be flipped by local spin operators. For example, for an α link ($\alpha = X, Y, Z$) between vertices i and j, α_i and α_j anticommute with vison parities at both plaquettes sandwiching the link (i, j) and commute with the vison parities at other hexagons. Therefore α_i and α_j can induce vison hoppings across the link (i, j). The Zeeman coupling ΔH in Eq. (2) involves a sum of all the local spin operators; as a result, it can also induce vison hopping across each link. Below we will illustrate how to extract the vison hopping amplitudes, induced by ΔH, from an example.

Let us consider an eigenstate of H from Eq. (1) consisting of two far-distant visons. We are interested in the "single-particle" properties of the visons; therefore we will take one of these visons simply as an auxiliary vison that is held immobile while the other is allowed to move [this can be accomplished by only acting with the perturbation ΔH from Eq. (2) within the region containing the mobile vison of

interest]. We place the immobile vison at a hexagon at $\mathbf{R}_0$ and consider fluctuations of the mobile vison within hexagon a, b, c, or d in Fig. 1(a). The *lowest*-energy eigenstate of H for each two-vison configuration is denoted as $|\Phi(\mathbf{R}_0, \mathbf{R}_l)\rangle$, with $l = a, b, c, d$. In the limit in which the two visons are much farther apart than the typical localization length of their Majorana zero modes, these four states will be degenerate. Moreover, when κ is finite, there will be a gap to all excitations, and therefore only those configurations that differ by changing the position of the vison will be connected by the perturbation ΔH. Under these conditions, one can then conceptualize these processes as coherent hopping of the vison particles. Then the leading in ΔH perturbative hopping amplitude of the vison from d to b (due to ΔH) is given by

$$t_{b,d} \equiv \langle \Phi(\mathbf{R}_0, \mathbf{R}_b)|\Delta H|\Phi(\mathbf{R}_0, \mathbf{R}_d)\rangle. \quad (4)$$

From the definition of the vison parity operator discussed above, one can see that only Y_2 and Y_4 anticommute with W_d and W_b while commuting with vison parities at all other hexagons. Therefore

$$t_{b,d} = -h_y \langle \Phi(\mathbf{R}_0, \mathbf{R}_b)|Y_2 + Y_4|\Phi(\mathbf{R}_0, \mathbf{R}_d)\rangle. \quad (5)$$

Similarly, it is straightforward to show the following expressions for the other hoppings:

$$t_{a,b} = -h_z \langle \Phi(\mathbf{R}_0, \mathbf{R}_a)|Z_3 + Z_2|\Phi(\mathbf{R}_0, \mathbf{R}_b)\rangle, \quad (6a)$$

$$t_{b,c} = -h_x \langle \Phi(\mathbf{R}_0, \mathbf{R}_b)|X_4 + X_5|\Phi(\mathbf{R}_0, \mathbf{R}_c)\rangle. \quad (6b)$$

Once the effective vison hopping for each link is obtained, one can extract the vison Berry phase acquired in a closed hopping associated with each closed path. For example, the phase acquired by hopping in the triangle $d \to b \to a \to d$ is defined as

$$\phi_{abd} = \text{Im} \ln(t_{d,a} t_{a,b} t_{b,d}), \quad (7)$$

and the phase acquired by hopping on the unit cell of translations $d \to c \to b \to a \to d$ is

$$\phi_{abcd} = \text{Im} \ln(t_{d,a} t_{a,b} t_{b,c} t_{c,d}). \quad (8)$$

If the phase ϕ_{abcd} acquired around a unit cell of the microscopic translational symmetries is not 0 (mod 2π), then the translations have a projective implementation on the vison particle [47,48]. As discussed in Refs. [37,40,49] for topologically ordered states with deconfined Z_2 gauge fields, this phase is expected to be either 0 or π, and its value is a robust topological characteristic of the phase as long as the the microscopic translational symmetry of the model is enforced. Notice, however, that these considerations do not apply to the phase ϕ_{abd} acquired around a single triangle, because this motion cannot be generated by the elements of the microscopic translation group, and therefore this phase can be sensitive to perturbations when only the translational symmetry is enforced.

The above formulas then define the mathematical problem at hand. The problem of computing these overlaps has been recently addressed in Ref. [36] employing the parton representation of spins. In the next section, we will, however, employ a different method that relies on an exact lattice duality developed in Ref. [37] building on the previous work of Refs. [38,40].
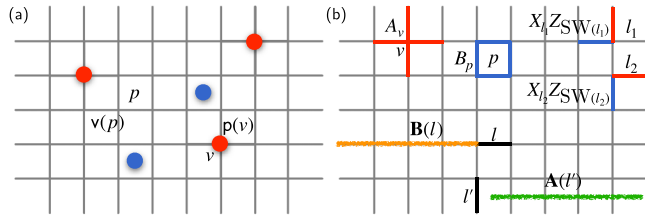
FIG. 2. (a) Schematic of a real-space configuration of the e (red dots) and ε (blue dots) particles. At each vertex v, there is a boson (e) mode with creation and annihilation operators $b_v^\dagger$ and b_v, respectively. Within each plaquette p, there is a complex fermion (ε) mode with creation and annihilation operators $c_p^\dagger$ and c_p, respectively, which is equivalent to two Majorana modes γ_p and γ_p'. (b) Spin operators and paths involved in the duality mapping. The Pauli X (Z) matrix at a link is represented by a red (blue) bond covering the link. For a vertical (horizontal) link l_1 (l_2), SW(l_1) [SW(l_2)] is the horizontal (vertical) link to its southwest which connects to it. The path $\mathbf{B}(l)$ (thick orange line) contains all the vertices to the left of a horizontal link l, and the dual lattice path $\mathbf{A}(l')$ (thick green line) contains all the plaquettes to the right of a vertical link l'.

B. Vison hoppings from the duality mapping

To use the duality mapping of Ref. [37], it is convenient to change the usual basis of the Kitaev model by performing a unitary transformation U. The transformation U *only* affects the spins from A-sublattice sites [see Fig. 1(a)]:

$$X_j \leftrightarrow Z_j, \quad Y_j \to -Y_j, \quad \forall j \in A. \quad (9)$$

The spin Hamiltonians in Eqs. (1) and (2) will be transformed accordingly, i.e., $H_K \to U H_K U^{-1} = \tilde{H}_K$, $\Delta H \to U \Delta H U^{-1} = \Delta \tilde{H}$:

$$\tilde{H}_K = K \left(\underbrace{\sum Z_i X_j}_{\substack{x \text{ link,} \\ i \in A}} - \underbrace{\sum Y_i Y_j}_{\substack{y \text{ link,} \\ i \in A}} + \underbrace{\sum X_i Z_j}_{\substack{z \text{ link,} \\ i \in A}} \right),$$

$$\Delta \tilde{H} = -\sum_{i \in A} (h_z X_i - h_y Y_i + h_x Z_i)$$

$$\qquad\quad - \sum_{j \in B} (h_x X_j + h_y Y_j + h_z Z_j), \quad (10)$$

and similarly for the κ term. In this new basis the vison parity reads as

$$W_d \to \tilde{W}_d = Z_4 Y_6 X_7 X_8 (-Y_1) Z_2$$
$$\qquad\qquad = X_6 X_7 X_8 X_1 Z_1 Z_2 Z_4 Z_6. \quad (11)$$

Therefore, by identifying the *sites* of the honeycomb lattice with the *links* of a square lattice as depicted in Fig. 1(b), this operator can be viewed as a product of the star (A_d) and plaquette ($B_{\mathsf{p}(d)}$) operators of the standard toric code model [50] [see Fig. 2(b)], as discussed in Refs. [37–40].

We will review here the exact duality mapping introduced in Ref. [37] for the case of an *infinite* system and refer the reader to Ref. [37] for details of the mapping on finite open and periodic lattices. The lattice duality allows us to map the tensor product Hilbert space of spins onto a tensor product Hilbert space of the "visons" and "spinons." The vison is a spinless hard-core boson which can viewed as being located

at the vertices of the square lattice [see Fig. 2(a)], analogous to the "e particles" of the toric code. Therefore we assign vison hard-core boson creation (annihilation) operators, $b_v^\dagger$ (b_v), with every vertex "v." The vison parity operator is then mapped as follows:

$$\tilde{W}_v \leftrightarrow e^{i\pi b_v^\dagger b_v}. \quad (12)$$

On the other hand, the spinon degrees of freedom correspond to those of a single spinless complex fermion mode per unit cell (which can be viewed as a descending of the "ε particle" of the toric code [37–40]). Therefore we introduce two spinon Majorana fermion modes, γ_p, γ_p' for every plaquette "p" of the lattice as depicted in Fig. 2(a). The fermion parity maps onto the following plaquette operator:

$$B_{\mathsf{p}(d)} = Z_1 Z_2 Z_4 Z_6 \leftrightarrow -i\gamma_{\mathsf{p}(d)}\gamma_{\mathsf{p}(d)}'. \quad (13)$$

Here, the operators $Z_1 \cdots Z_6$ are those appearing in the usual plaquette term of the toric code, and $\mathsf{p}(d)$ stands for the plaquette to the *northeast* of vertex d, as depicted in Fig. 1(b). We can combine the Majorana modes into complex fermion operators as follows:

$$c_p = (\gamma_p + i\gamma_p')/2, \quad c_p^\dagger = (\gamma_p - i\gamma_p')/2. \quad (14)$$

Note that $-i\gamma_p\gamma_p' = e^{i\pi c_p^\dagger c_p}$.

We will now present the "dictionary" that allows us to map exactly any local operator acting on the underlying physical spin degrees of freedom onto operators acting on the dual vison and spinon degrees of freedom, introduced in Ref. [37]. The mapping of spin operators on a link l is as follows.

(i) For vertical l,

$$Z_l \leftrightarrow (b_{v_1} + b_{v_1}^\dagger)(b_{v_2} + b_{v_2}^\dagger)e^{i\pi\alpha_l}, \quad (15a)$$

$$X_l Z_{\text{SW}(l)} \leftrightarrow i\gamma_{p_1}\gamma_{p_2}'. \quad (15b)$$

(ii) For horizontal l,

$$Z_l \leftrightarrow (b_{v_1} + b_{v_1}^\dagger)(b_{v_2} + b_{v_2}^\dagger), \quad (16a)$$

$$X_l Z_{\text{SW}(l)} \leftrightarrow e^{i\pi\beta_l}i\gamma_{p_1}\gamma_{p_2}'. \quad (16b)$$

Here,

$$\alpha_l = \sum_{p \in \mathbf{A}(l)} c_p^\dagger c_p, \quad \beta_l = \sum_{v \in \mathbf{B}(l)} b_v^\dagger b_v. \quad (17)$$

Here, for a vertical (horizontal) link l, v_1 and v_2 are the two vertices connected by it, while p_1 and p_2 are the two plaquettes at the left and right (top and bottom) sides of it; SW(l) is the link to the southwest of l which also connects to it [see Fig. 2(b)]. Also, $\mathbf{A}(l)$ [$\mathbf{B}(l)$] denotes sets of plaquettes (vertices) that reside on a string in the dual (direct) lattice; $\mathbf{A}(l)$ and $\mathbf{B}(l)$ are depicted in Fig. 2(b). These "string" operators are the ones encoding the attribute that the vison and the spinon have nonlocal statistical interactions that make them behave as mutual semions. Notice that the spin operators described above form a complete algebraic basis out of which any other operator can be obtained by taking sums, products, and multiplication by complex numbers, from this basis.

In particular, we can apply the above dictionary to rewrite the Hamiltonian from Eq. (10) in terms of vison and spinon

degrees of freedom, leading to

$$\tilde{H} = K \sum_p [e^{i\pi \beta_{L(p,p+\hat{y})}}(i\gamma_{p+\hat{y}}\gamma'_p + i\gamma_{p+\hat{y}}\gamma'_{p+\hat{x}}) + i\gamma_p\gamma'_{p+\hat{x}}]$$

$$- \kappa \sum_p [e^{i\pi \beta_{L(p,p+\hat{y})}}(i\gamma_{p+\hat{y}}\gamma_{p-\hat{x}}) + e^{i\pi b^\dagger_{\mathsf{v}(p)}b_{\mathsf{v}(p)}}(i\gamma_{p-\hat{x}}\gamma_p) + e^{i\pi \beta_{L(p,p+\hat{y})}}(i\gamma_p\gamma_{p+\hat{y}})$$

$$+ e^{i\pi \beta_{\tilde{L}(p-\hat{x},p-\hat{x}+\hat{y})}}(i\gamma'_{p+\hat{y}}\gamma'_p) + i\gamma'_{p+\hat{x}}\gamma'_p + e^{i\pi \beta_{\tilde{L}(p,p-\hat{y})}}(i\gamma'_{p-\hat{y}}\gamma'_{p+\hat{x}})]. \tag{18}$$

Here, $\mathsf{v}(p)$ denotes the vertex to the *southwest* of plaquette p [see Fig. 2(a)], and $\tilde{L}(p, p')$ stands for the link sandwiched by plaquettes p and p'. Notice that the above Hamiltonian explicitly commutes with the vison occupation of all the vertices in

the lattice and the remaining dynamical degrees freedom are described by a fermion bilinear model, as expected.

On the other hand, one can show that the $\Delta\tilde{H}$ in Eq. (10) can be rewritten as

$$\Delta\tilde{H} = - \sum_v [h_z(b_v + b^\dagger_v)(b_{v+\hat{x}} + b^\dagger_{v+\hat{x}})(1 + i\gamma_{\mathsf{p}(v)}\gamma'_{\mathsf{p}(v)+\hat{x}}) + h_y(b_{v-\hat{x}} + b^\dagger_{v-\hat{x}})(b_{v+\hat{y}} + b^\dagger_{v+\hat{y}})(\gamma_{\mathsf{p}(v)-\hat{x}}\gamma'_{\mathsf{p}(v)})e^{i\pi\alpha_{L(v,v+\hat{y})}}$$

$$+ h_y e^{i\pi \beta_{L(v+\hat{y},v+\hat{y}+\hat{x})}}(b_v + b^\dagger_v)(b_{v+\hat{x}+\hat{y}} + b^\dagger_{v+\hat{x}+\hat{y}})(-\gamma_{\mathsf{p}(v)+\hat{y}}\gamma'_{\mathsf{p}(v)})e^{i\pi\alpha_{L(v,v+\hat{y})}}$$

$$+ h_x(e^{i\pi \beta_{L(v+\hat{y},v+\hat{y}+\hat{x})}}i\gamma_{\mathsf{p}(v)+\hat{y}}\gamma'_{\mathsf{p}(v)} + 1)(b_v + b^\dagger_v)(b_{v+\hat{y}} + b^\dagger_{v+\hat{y}})e^{i\pi\alpha_{L(v,v+\hat{y})}}]. \tag{19}$$

Here, $L(v, v')$ stands for the link connecting vertices v and v'. As we see, the Zeeman term contains vison hopping and pair creation terms, creating an impediment to solving it exactly.

Therefore our strategy is to treat $\Delta\tilde{H}$ as a perturbation acting on the exact eigenstates of Eq. (18). Let us discuss how to uniquely label these states. An eigenstate of Eq. (18) with N visons placed in the vertices $\{v_1, \dots, v_N\}$ can be written as a tensor product of vison and spinon degrees of freedom as follows:

$$b^\dagger_{v_1} \cdots b^\dagger_{v_N}|0\rangle \otimes |\Psi^\varepsilon(\mathbf{R}_1, \dots, \mathbf{R}_N)\rangle, \tag{20}$$

where $\mathbf{R}_i$ denotes the position of vertex v_i. The first term specifies the vison locations, and the second term is the fermionic spinon wave function resulting from diagonalizing the effective Bogoliubov–de Gennes (BdG) Hamiltonian $H^\varepsilon(\mathbf{R}_1, \dots, \mathbf{R}_N)$ associated with Eq. (18). Notice that this Hamiltonian has already a unique specified gauge choice for the vector potential that captures the long-range statistical interaction after the vison occupations are given and viewed as constants. We caution that the tensor product structure above is in a dual Hilbert space and does not have a simple relation to the tensor structure of the underlying physical spin degrees of freedom (see Ref. [37] for further discussions).

Let us now specialize to the case of two visons to compute the matrix elements described in Eqs. (4), (5), (6a), and (6b). These vison hopping elements can then be systematically computed. For example, the hopping between vertices a and b [see Fig. 1(b)] can be obtained as follows:

$$t_{a,b} = - h_z\langle 0|b_0 b_a \otimes \langle\Psi^\varepsilon_0(\mathbf{R}_a, \mathbf{R}_0)|(b_a + b^\dagger_a)(b_b + b^\dagger_b)$$

$$\times (1 + i\gamma_{\mathsf{p}(a)}\gamma'_{\mathsf{p}(b)}) b^\dagger_b b^\dagger_0|0\rangle \otimes |\Psi^\varepsilon_0(\mathbf{R}_b, \mathbf{R}_0)\rangle$$

$$= - h_z\langle\Psi^\varepsilon_0(\mathbf{R}_a, \mathbf{R}_0)|(1 + i\gamma_{\mathsf{p}(a)}\gamma'_{\mathsf{p}(b)})|\Psi^\varepsilon_0(\mathbf{R}_b, \mathbf{R}_0)\rangle. \tag{21}$$

Here, $|\Psi^\varepsilon_0(\mathbf{R}_j, \mathbf{R}_0)\rangle$ is the *lowest*-energy eigenstate of $H^\varepsilon(\mathbf{R}_j, \mathbf{R}_0)$. Similarly, the hopping between vertices a and d reads

$$t_{d,a} = - h_x\langle\Psi^\varepsilon(\mathbf{R}_d, \mathbf{R}_0)|(1 + i\gamma_{\mathsf{p}(a)}\gamma'_{\mathsf{p}(d)})e^{i\pi\alpha_{L(a,d)}}$$

$$\times |\Psi^\varepsilon(\mathbf{R}_a, \mathbf{R}_0)\rangle. \tag{22}$$

Here, $e^{i\alpha_{L(a,d)}}$ reflects the statistical interaction between visons and spinons, and we have assumed that the vertex 0 is in the same row as vertex d.

We would like to briefly comment on the duality mapping for the case of a periodic system, which is the geometry that we use for the numerical implementation to be described in the next section. There are two global constraints on a torus:

$$\prod_v \tilde{W}_v = 1, \quad \prod_p B_p = 1. \tag{23}$$

Therefore only states with an *even* number of visons and spinons are physical in the torus. Moreover, there are additionally two global Wilson loop degrees of freedom associated with the noncontractible loops around the torus. For the exactly solvable model where the visons are static, the topological degrees of freedom associated with the Wilson loops can be taken to be two quantum numbers with values $z_{1,2} = +1$ ($z_{1,2} = -1$) that specify whether the spinons have periodic (antiperiodic) boundary conditions along the x or y directions of the torus (z_1 and z_2 are for the x and y directions, respectively). Therefore the fermionic BdG eigenstates are labeled as $|\Psi^\varepsilon_0(\mathbf{R}_j, \mathbf{R}_0; z_1, z_2)\rangle$. The vison hoppings can then be calculated in the same way as shown in Eqs. (21) and (22). More details regarding the duality mapping on a torus can be found in Ref. [37].

In the next section, we will discuss the results with $(z_1, z_2) = (-1, -1)$, i.e., antiperiodic boundary conditions (APBCs) for ε particles. The results with periodic bound-
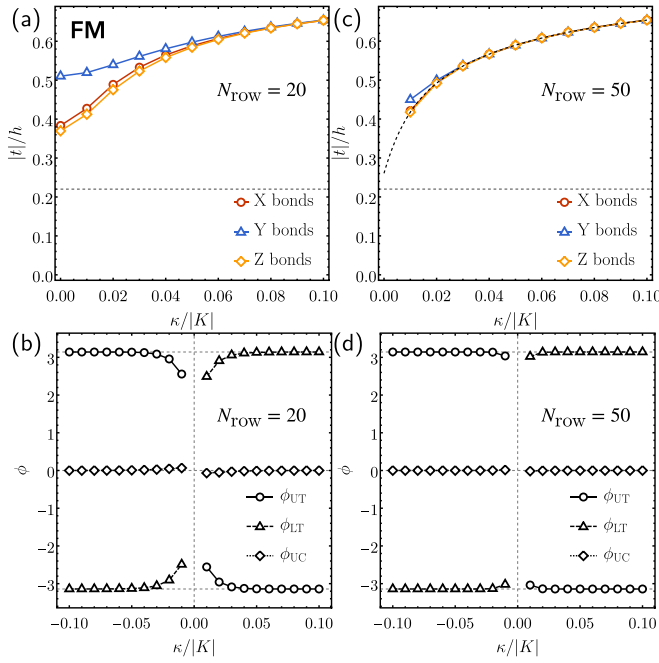
FIG. 3. The vison hopping amplitude and Berry phases with FM coupling. (a) Hopping amplitudes with system size $N_{\rm row} = 20$. (b) The Berry phases associated with two minimal triangles and the plaquette path. (c) and (d) The same as in (a) and (b), but for $N_{\rm row} = 50$. The magnitude of the hopping is independent of $\operatorname{sgn}(\kappa) = \operatorname{sgn}(h_x h_z h_y)$; therefore we only present results for positive κ. The amplitudes have been normalized for a Zeeman field along the [111] direction, $h_x = h_y = h_z = h/\sqrt{3}$, but the hoppings for other directions of the Zeeman field can be easily estimated from the above plots by rescaling using Eqs. (5)–(8).

FIG. 4. The vison hopping amplitude and Berry phases with AFM coupling. (a) The hopping amplitude with system size $N_{\rm row} = 20$. (b) The Berry phases associated with two minimal triangles and the plaquette. (c) and (d) The same as in (a) and (b), but for $N_{\rm row} = 50$. The inset of (c) is a log-log plot of the same data, which suggests $|t_\alpha| \approx 0.55|h_\alpha|\,|\kappa/K|^\nu$ with $\nu \approx 0.5$, when the vison hops across an α bond, with $\alpha \in \{X, Y, Z\}$ (see Fig. 1). Notice that the vison phases on the triangles depend on $\operatorname{sgn}(\kappa) = \operatorname{sgn}(h_x h_z h_y)$. We use the same the conventions for phases and for normalizing hoppings as in Fig. 3.

ary conditions (PBCs) [$(z_1, z_2) = (1, 1)$] are presented in Appendix A.

IV. VISON HOPPINGS AND BERRY PHASES

A. Results for FM and AFM couplings

As the expressions in Eqs. (21) and (22) illustrate, the calculation of the vison hopping amplitudes and Berry phases has been reduced to a problem of computing matrix elements of operators between free-fermion BCS ground states. The mathematical details as to how to compute these matrix elements have been discussed in Refs. [37,51], and we will here present results following the same approach as in Ref. [37]. All the numerical results that we will show have been calculated for the square torus: $N_{\rm row} = N_{\rm col}$. For the plots that we will present we have taken the Zeeman field along the [111] direction, so that $h_x = h_y = h_z = h/\sqrt{3}$. Nevertheless, the vison hoppings for other directions of the Zeeman field can be easily estimated from Figs. 3 and 4 via a rescaling using Eqs. (5)–(8) and keeping track of the corresponding change in $\kappa \approx h_x h_y h_z / K^2$.

Figure 3 shows the results for the FM Kitaev model at two different system sizes: $N_{\rm row} = 20$ in Figs. 3(a) and 3(b) and $N_{\rm row} = 50$ in Figs. 3(c) and 3(d). The hoppings are labeled according to the type of bonds crossed by the vison, e.g., $t_{a,b} \in Z$ bonds, $t_{b,d} \in Y$ bonds, and $t_{d,a} \in X$ bonds [see Fig. 1(a)].
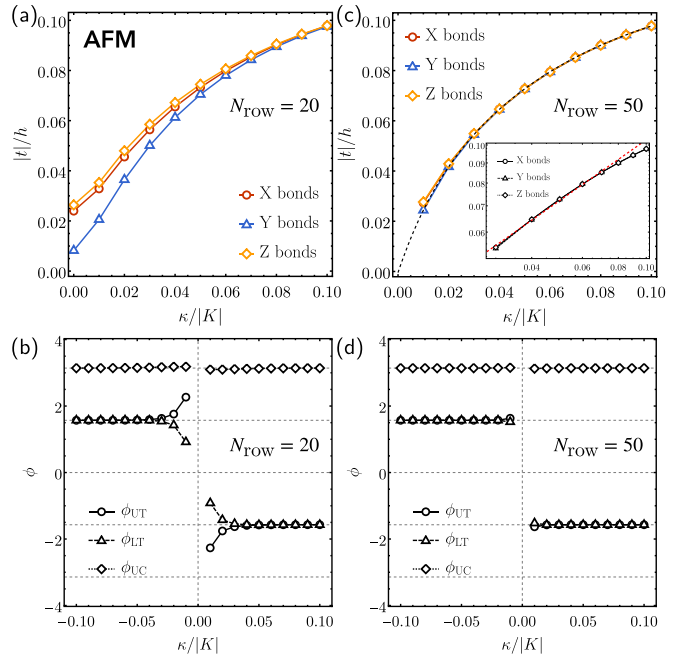
Our results are consistent with the expected symmetry of the honeycomb lattice according to which the magnitudes of the hopping amplitude on all bonds are the same in the thermodynamic limit ($N_{\rm row} \to \infty$); however, the convergence degrades and becomes slower as the fermion gap vanishes for $\kappa \to 0$, as evidenced by contrasting the behavior of $N_{\rm row} = 20$ with that of $N_{\rm row} = 50$ in Fig. 3 and as further discussed in Appendix B [52]. Moreover, we have observed that for a strict value of $\kappa = 0$ the vison hoppings are sensitive to the choice of fermion boundary conditions [Wilson loop sectors (z_1, z_2)], further indicating that the vison hopping may not be well defined in the $\kappa = 0$ case (see Appendix A for more details). The horizontal dashed lines in Figs. 3(a) and 3(c) indicate the result of Ref. [36] for the magnitude of the hopping; in Ref. [36] all calculations were performed strictly at $\kappa = 0$. We see that our extrapolation to $\kappa \to 0$ at $N_{\rm row} = 50$ [dashed curve in Fig. 3(c)] is in agreement with Ref. [36] and is given by $|t_\alpha| \sim 0.38|h_\alpha|$, when the vison hops across an α bond, with $\alpha \in \{X, Y, Z\}$ (see Fig. 1).

The phases for the FM model are shown in Figs. 3(b) and 3(d), for a vison hopping around an upper triangle $\phi_{\rm UT}$ ($d \to b \to a \to d$ in Fig. 1), a lower triangle $\phi_{\rm LT}$ ($d \to c \to b \to d$ in Fig. 1), and a Bravais unit cell $\phi_{\rm UC}$ ($d \to c \to b \to a \to d$ in Fig. 1). We see clear evidence that for $\kappa \neq 0$ these phases approach the following values in the thermodynamic limit:

$$\phi_{\rm LT} = -\phi_{\rm UT} = \pi \operatorname{sgn}(\kappa) = \pi \quad (\text{FM}), \tag{24a}$$

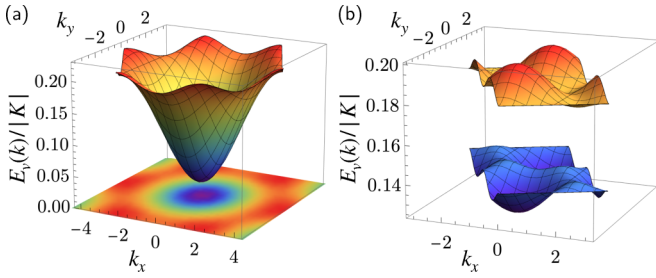$$\phi_{\rm UC} = 0 \quad (\text{FM}), \tag{24b}$$

FIG. 5. The vison bands for FM (a) and AFM (b) couplings at small Zeeman fields. The triangular lattice's lattice constant is set to be $a = 1$. (a) The bands for FM coupling with $h = 0.1|K|$, and so $\kappa/|K| = (h/\sqrt{3})^3/|K|^3 \sim 10^{-4}$ according to perturbation theory [1]. The single-vison excitation energy is found to be $E_0 \approx 0.15|K|$. (b) The bands for AFM coupling with $\kappa/K = (h/\sqrt{3}K)^3 = 0.01$. For this κ, the single-vison excitation energy is $E_0 \approx 0.16K$ (obtained for $N_{\mathrm{row}} = 30$). Note that for the FM Kitaev model, the vison band has a larger width and its band minimum is closer to zero.
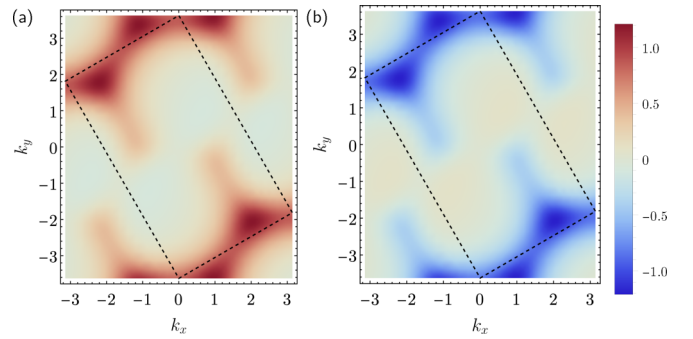

FIG. 6. Berry curvature of the upper (a) and lower (b) vison bands in Fig. 5(b). The black dashed rectangle indicates the reduced Brillouin zone. The Chern number of the upper (lower) band is $+1$ (-1).

where in the last equality of Eq. (24a) we have used the fact that phases are defined modulo 2π. The above is one of our central findings: The vison in the FM model acquires zero phase around a unit cell of the Bravais lattice, and thus translations act in a nonprojective fashion.

The results for the AFM coupling are shown in Fig. 4. Interestingly, we find that the hopping amplitude approaches 0 as $\kappa \to 0$ in the thermodynamic limit, in agreement with Ref. [36]. Even more remarkably, for nonzero κ, our results are approaching the following values of the phases around triangles and the unit cell in the thermodynamic limit:

$$\phi_{\mathrm{LT}} = \phi_{\mathrm{UT}} = -\frac{\pi}{2}\operatorname{sgn}(\kappa) \quad \text{(AFM)}, \tag{25a}$$

$$\phi_{\mathrm{UC}} = \pi \quad \text{(AFM)}. \tag{25b}$$

Therefore we see that the vison acquires phase π when moving around a unit cell, and therefore translations need to be implemented projectively. Similarly to the FM case, in the AFM model at $\kappa = 0$ we also observe strong sensitivity to the spinon boundary conditions and system sizes (see Appendix A for more details).

B. Vison Chern bands

From the effective vison hoppings computed in the previous section we can construct the vison band dispersions for both FM and AFM couplings. For FM coupling, the vison does not experience flux within the unit cell ($\phi_{\mathrm{UC}} = 0$), and therefore the vison band is simply that of a single-site nearest-neighbor tight-binding model in the triangular lattice. As a consequence this band has no Berry curvature. Figure 5(a) shows the vison band dispersion at $h = 0.1|K|$, $\kappa/|K| = (h/\sqrt{3}K)^3 \sim 10^{-4}$, which has a small gap.

On the other hand, for the AFM model, $\phi_{\mathrm{UT}} = \phi_{\mathrm{LT}} = -\pi/2\operatorname{sgn}(\kappa)$ and $\phi_{\mathrm{UC}} = \pi$. Therefore the vison unit cell needs to be doubled, giving rise to two vison bands. Figure 5(b) shows the vison bands at $\kappa/K = (h/\sqrt{3}K)^3 = 0.01$. We have also calculated the Berry curvature and Chern number for each band. Interestingly, we found that both bands have a nontrivial topology; the higher (lower) band has a Chern

number $C = +1$ ($C = -1$). The Berry curvatures for the two bands are shown in Fig. 6.

V. CONSISTENCY CHECK OF VISON PHASES VIA COMMUTING PROJECTOR HAMILTONIANS

In this section we would like to offer some supporting evidence that the phases that the vison acquires around a unit cell are indeed 0 and π for the FM and AFM Kitaev models, respectively. Currently, we do not know any method allowing us to compute these phases purely analytically when the fermionic Majorana spinons are forming a topological superconducting state with a nonzero BdG Chern number $C \neq 0$. Nevertheless, as argued in Ref. [40], when the Majorana spinons have zero Chern number ($C = 0$), the phase that the vison acquires around each unit cell can indeed be computed analytically thanks to the fact that the state can be adiabatically deformed into the ground state of a Hamiltonian made out of sums of commuting projectors (like the toric code), and such adiabatic deformation can be performed without breaking the lattice translational symmetry of the model.

To exploit this idea, we will add a term to the Hamiltonian that drives a phase transition into a state with vanishing spinon Chern number ($C = 0$) that can be described with commuting projector Hamiltonians. By following the discussion of Ref. [40], we will select this commuting projector state such that the vison still acquires the same phase around a unit cell as in the original state of interest with nonzero C. By explicitly verifying that the phase of the vison around a plaquette indeed does not change across such a phase transition, we will be able to clearly confirm that the values of the vison phases that we have computed numerically agree with those of the simpler commuting projector Hamiltonian state.

However, what are these ideal commuting projector states? As discussed in Refs. [40,53–55], the gapped paired BCS states of fermionic spinons with translational symmetry can be classified by the Chern number $C \in \mathbb{Z}$ and by four parity indices $\zeta_k = \pm 1$, associated with the four special high-symmetry points (HSPs) of the Brillouin zone: $\{(0,0),(0,\pi),(\pi,0),(\pi,\pi)\}$. The value $\zeta_k = -1$ (1) is viewed as nontrivial (trivial), and it indicates that the ground state has an odd (even) number fermions occupying the special momentum k state (if such a k state is allowed by the boundary
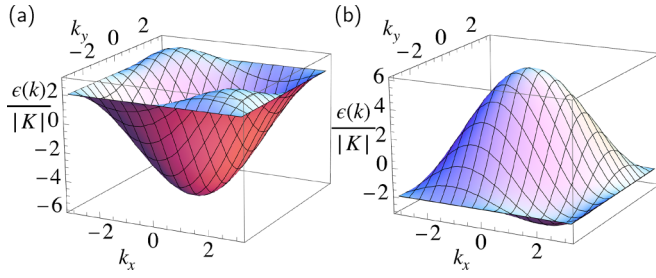
FIG. 7. Number-conserving part of ε-particle bands (on a square lattice) from $\tilde{H}$ with FM (a) and AFM (b) couplings. The lattice constant is set to be 1.

conditions and the size of the system). The Chern number and these parity indices are related as follows:

$$(-1)^C = \zeta_{(0,0)}\zeta_{(0,\pi)}\zeta_{(\pi,0)}\zeta_{(\pi,\pi)}. \qquad (26)$$

The states with the commuting projector Hamiltonians in which we are interested have $C = 0$ and either all the parity indices taking the trivial value ($\zeta_k = 1$) or all taking the nontrivial value ($\zeta_k = -1$) [56]. Among these states the one with all four parity indices being trivial ($\zeta_k = 1$) and $C = 0$ is adiabatically connected to a trivial "atomic insulator" vacuum of fermionic spinons, namely, the state of the spinon is completely empty, which is essentially a toric code vacuum state, which we label TC-AI$_0$ [57]. As discussed in Refs. [37,40], this state is adiabatically equivalent to the ground state of the usual toric code, and the vison in this case is simply the usual e particle, which clearly acquires 0 phase when moving around a unit cell.

On the other hand, the states with $\zeta_k = -1$ for all four HSPs are adiabatically connected to another trivial "atomic insulator" state, with one ϵ spinon per unit cell, which is the analog of a fully occupied toric code state, which we label TC-AI$_1$ [58]. The ideal commuting projector Hamiltonians in this case are the toric code model but with the opposite sign for both the vertex and plaquette couplings, so that every plaquette contains an ε particle [37,39,40]. It is straightforward to verify that the vison (e particle) in this state will acquire a π flux when encircling a unit cell, simply because each unit cell contains an ε particle, which is a semion relative to the e particles.

By following the ideas of Ref. [37], we will now show that the vison in the FM Kitaev model is expected indeed to have the same phases as in the trivial atomic insulator of spinons TC-AI$_0$, namely, $\phi_{UC} = 0$, whereas the vison of the AFM Kitaev model has the same phase as in the trivial atomic insulator TC-AI$_1$, i.e., $\phi_{UC} = \pi$. The ε particle's band dispersion (obtained from the number-conserving part of the ε-particle Hamiltonian) for H with FM and AFM couplings is shown in Figs. 7(a) and 7(b), respectively. For FM coupling, $\epsilon(0,0) = -6|K|$, $\epsilon(\pi,0) = \epsilon(0,\pi) = \epsilon(\pi,\pi) = 2|K|$, and thus $\zeta_{(0,0)} = -1$ and $\zeta_k = +1$ for the rest of the HSPs. Its parity indices at the four HSPs are closer to those of the TC-AI$_0$ state, so we expect $\phi_{UC} = 0$ [59]. As for AFM coupling, the ε band dispersion is simply opposite to that of the FM case. The parity indices $\zeta_{(0,0)} = 1$ and $\zeta_k = -1$ at the other HSPs, which values are closer to those of the TC-AI$_1$ state. Therefore we expect $\phi_{UC} = \pi$ from the arguments of Ref. [37].
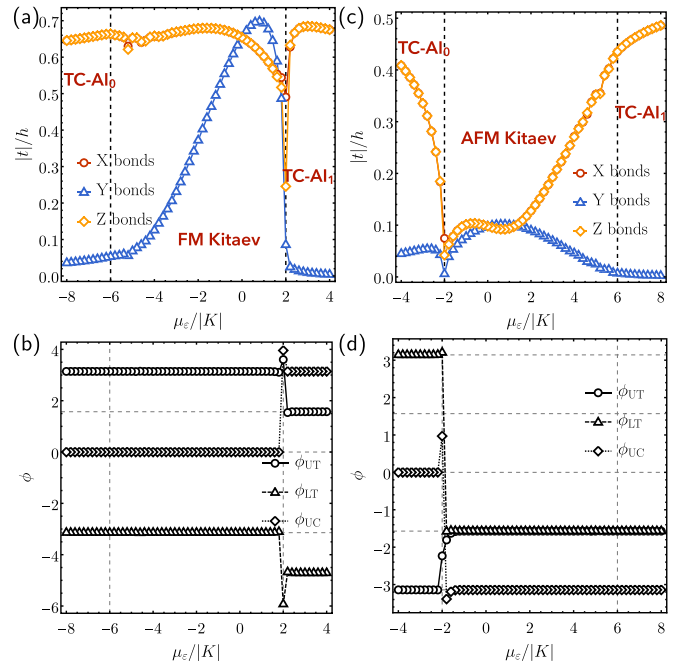

FIG. 8. Vison hopping as a function of μ_ε at $\kappa/|K| = 0.1$. (a) and (b) The hopping amplitude and ϕ for FM coupling. (c) and (d) The same as (a) and (b), but for AFM coupling. Calculations are done with $N_{\text{row}} = 50$ and APBCs.

We will now provide direct numerical evidence for the above expected values of ϕ_{UC} in the FM and AFM Kitaev models. To do so, we add the following additional term H_1 into H, which reads (after the unitary transformation U introduced in Sec. III B)

$$UH_1U^{-1} = \sum_p \frac{\mu_\varepsilon}{2}\left(\prod_{l\in\text{boundary}(p)} Z_l - 1\right). \qquad (27)$$

Here, p stands for a plaquette in the square lattice [see Fig. 1(b)]. Under the duality mapping discussed in Sec. III B and in Ref. [37], the above term is mapped into $\sum_p -\mu_\varepsilon c_p^\dagger c_p$. Therefore this term simply introduces a chemical potential to ε particles, and therefore it naturally drives the ground state into the commuting projector limit of the TC-AI$_0$ state when μ_ε is sufficiently negative and into the commuting projector limit of the TC-AI$_1$ state when μ_ε is sufficiently positive. We calculated the phase that the vison acquires around a unit cell, ϕ_{UC}, at different κ and μ_ε. Figure 8 shows the result for $\kappa/|K| = 0.1$ with both FM and AFM Kitaev couplings. For FM coupling [Figs. 8(a) and 8(b)], as μ_ε is tuned to the band edges, the vison hopping crossing Y bonds decreases while the hoppings crossing X and Z bonds are approaching ~ 0.7. When $-6|K| \leqslant \mu_\varepsilon \leqslant 2|K|$, $\zeta_{(0,0)} = -1$ and $\zeta_k = 1$ for the other three HSPs, and the parity indices' configuration is closer to that of the TC-AI$_0$ state. Indeed, the vison phase ϕ_{UC} is always 0 in this regime. When $\mu_\varepsilon < -6|K|$, since the bare ε band is empty ($\zeta_k = 1$ at all four HSPs), the ε ground state is adiabatically connected to the TC-AI$_0$ state and $\phi_{UC} = 0$. Therefore ϕ_{UC} does not change its value across this FM-Kitaev to TC-AI$_0$ transition. On the other hand, when μ_ε becomes larger than $2|K|$, ϕ_{UC} suddenly jumps to π. This
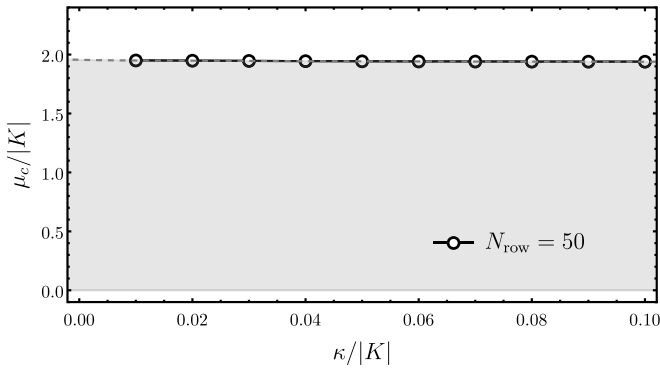
FIG. 9. Critical μ_c for the 0 to π jump of ϕ_{UC} at different κ with FM coupling. $N_{\mathrm{row}} = 50$. $\phi_{\mathrm{UC}} = 0$ in the gray region with the caveat that ϕ_{UC} at strictly $\kappa = 0$ could be ill defined.

can be understood from the fact that in this regime, $\zeta_k = -1$ for all HSPs and the ε ground state is adiabatically connected to TC-AI$_1$; so ϕ_{UC} should take the same value as that of the TC-AI$_1$ state. For AFM coupling [Figs. 8(c) and 8(d)], as μ_ε is tuned to the band edge, the vison hoppings crossing X and Z bonds are close to $\sim 0.5|h|$ while the hopping across Y bonds decreases. For $-2|K| \leqslant \mu_\varepsilon \leqslant 6|K|$, $\zeta_{(0,0)} = 1$ while ζ_k at all the other three HSPs is -1, which values are closer to those of the TC-AI$_1$ state. Indeed, we found that ϕ_{UC} is always π across the AFM-Kitaev to TC-AI$_1$ ($\mu_\varepsilon \geqslant 6|K|$) transition. On the other hand, when the ε ground state enters the TC-AI$_0$ regime ($\mu_\varepsilon < -2|K|$), ϕ_{UC} jumps to 0. Therefore our results indicate that the vison phase ϕ_{UC} for FM (AFM) Kitaev coupling is indeed the same as that of the TC-AI$_0$ (TC-AI$_1$) state, as expected from the considerations of Ref. [37]. Moreover, we have performed the same type of calculations at smaller κ values; for each κ, we found a similar 0 to π jump behavior at some "critical" chemical potential μ_c. Figure 9 shows the result for μ_c at different κ values with a FM coupling. It can be seen that μ_c is not sensitive to κ at small κ values; this can be understood from the perspective of our conjecture as κ does not affect the number-conserving part (hopping and chemical potential) of ε particles' Hamiltonian, and therefore ζ_k at all four HSPs are independent of κ. Below the μ_c-κ curve (the gray region in Fig. 9), there is always $\phi_{\mathrm{UC}} = 0$. Note that although the extrapolation of results with finite κ tends to suggest $\phi_{\mathrm{UC}} = 0$ for the $\kappa = 0$ FM Kitaev model ($\mu_\varepsilon = 0$), due to the reasons described previously, ϕ_{UC} at $\kappa = 0$ may not be a well-defined quantity.

VI. SUMMARY AND DISCUSSION

Using a recently developed exact duality mapping [37] that allows us to rewrite the microscopic spin operators in terms of nonlocal vison and fermionic spinon degrees of freedom, we have investigated the nature of the motion of the emergent flux carrying vison particles in the Kitaev honeycomb model perturbed by a Zeeman field. This Zeeman field not only induces the well-known Haldane-type mass gap on the itinerant Majorana fermions, but also induces vison hopping, breaking the exact solvability of the model.

We have seen that while the FM ($K < 0$) and AFM ($K > 0$) Kitaev models have the same non-Abelian Ising topological order, they are sharply distinct phases of matter when viewed as topologically ordered states that are enriched by the discrete translational symmetry of the honeycomb lattice. As a consequence of this, the nature of the motion of the vison particle is sharply distinct in the FM vs the AFM Kitaev honeycomb models. For example, in the FM Kitaev model the vison acquires a trivial phase when it encircles a unit cell of the honeycomb Bravais lattice: $\phi_{\mathrm{UC}} = 0$. Since there is a single vison site per unit cell (which can be viewed as being located at the center of the plaquette), this implies that the vison moves effectively in a single-site triangular lattice with zero flux. There is therefore a single vison band which has zero Berry curvature and thus no associated intrinsic contribution to the thermal Hall effect. To further back up this conclusion, we have shown that the vison phase around the unit cell remains unchanged across a phase transition into another ground state that is adiabatically connected to the ground state of the standard toric code model, which is a commuting projector Hamiltonian where this phase can be computed fully analytically and where it is clear that translations act nonprojectively on its anyon excitations.

On the other hand, in the AFM Kitaev model the vison acquires a nontrivial phase when it hops around a unit cell: $\phi_{\mathrm{UC}} = \pi$. As a consequence, lattice translations are implemented projectively on the vison, and the vison unit cell needs to be doubled. In this case, the vison has two separate bands with nonzero Chern numbers $C = \pm 1$ and an associated contribution to the intrinsic thermal Hall effect.

There are also crucial energetic differences between the vison bands in the FM and AFM models. In the FM model, the magnitude of the vison hopping and bandwidth grow linearly with the Zeeman field, $|t_\alpha| \approx 0.38|h_\alpha|$, when the vison hops across an α bond ($\alpha = X, Y, Z$; see Fig. 1) at the leading perturbative order, which agrees with the value reported in Ref. [36]. For the AFM model our results are consistent with a vanishing leading perturbative hopping of the vison that is linear in Zeeman fields, as also reported in Ref. [36]. However, we have seen that in the presence of the Haldane mass term of the Majorana fermions, $\kappa \approx h_x h_y h_z / K^2$ [1], the magnitude of the vison hopping becomes nonzero and scales as $|t_\alpha| \propto |h_\alpha||\kappa/K|^\nu$ when the vison hops across an α bond ($\alpha \in \{X, Y, Z\}$; see Fig. 1), with $\nu \approx 0.5$ at small κ and h_α. As a consequence of this, the visons in the FM model are substantially more mobile at small values of the Zeeman field than in the AFM model. Therefore the Zeeman field is expected to destabilize more easily the FM Kitaev spin liquid via vison gap closing and condensation, relative to the AFM Kitaev spin liquid. This is naturally consistent with a variety of numerical studies which have reported that the FM Kitaev spin liquid is more fragile than the AFM Kitaev spin liquid against a Zeeman field (see, e.g., Refs. [24–27]). While the single-vison gap-closing picture found here provides a natural mechanism for an instability of the Kitaev spin liquid, it should be noted that such a proliferation mechanism can also be applied to tightly bounded vison pairs. As discussed in Refs. [60,61], a bounded vison pair also gains dynamics under perturbations such as a Zeeman field and Heisenberg and gamma inter-
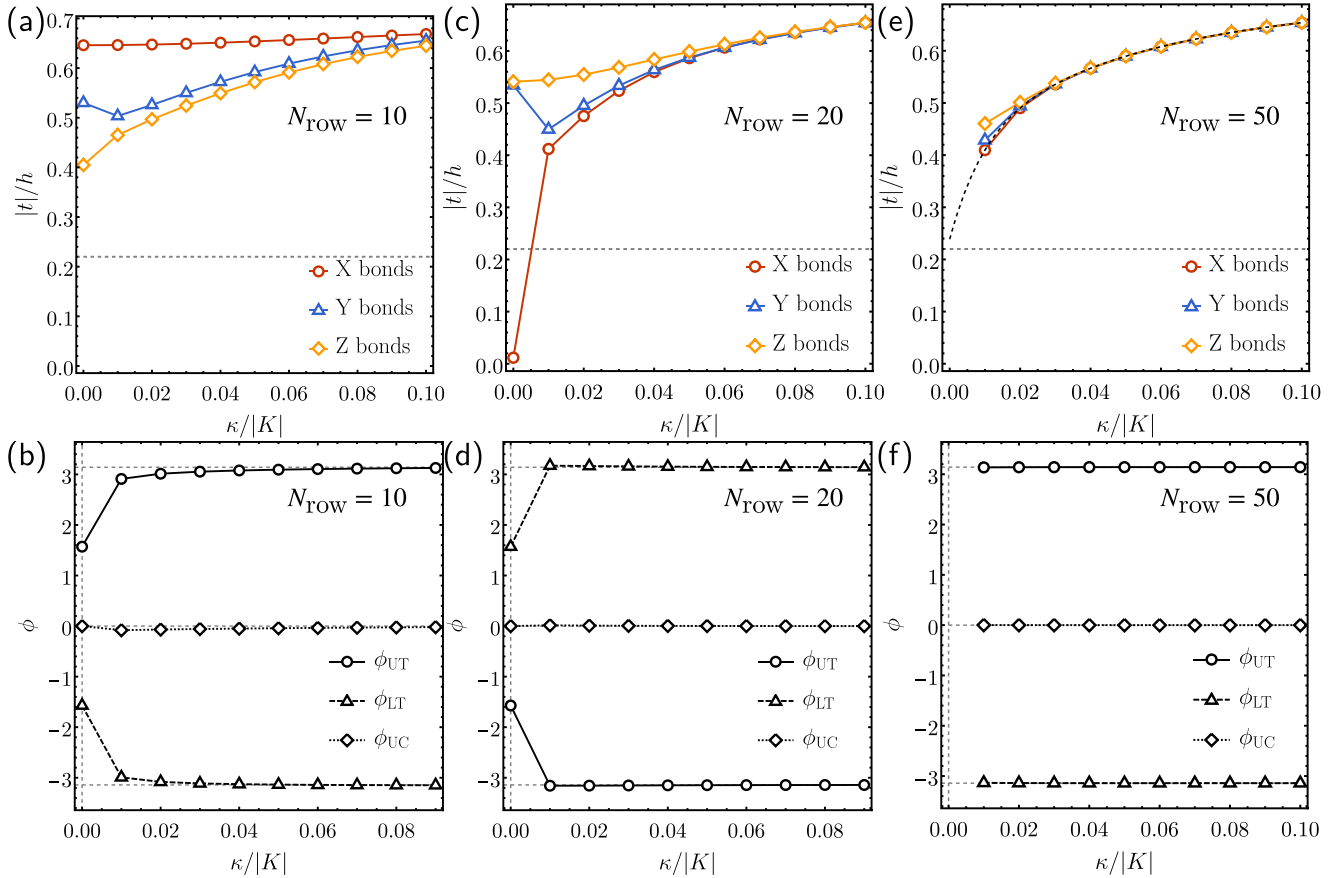
FIG. 10. (a)–(f) The vison hopping amplitude and ϕ with FM coupling at selected system sizes with PBCs for the spinons. The results at finite κ are consistent with the APBC data presented in the main text, whereas at $\kappa = 0$, the hoppings across certain bonds can be dropped to very small values, which causes an ambiguity in determining the vison Berry phases.

actions. According to the magnitude of induced vison-pair hopping amplitudes, in Refs. [60,61] it was reported that the FM (AFM) Kitaev spin liquid is more robust (fragile) against Heisenberg interaction and fragile (robust) against a Zeeman field and gamma interaction, in agreement with our findings.

While the precise relation between the ideal spin liquids realized in the weakly perturbed Kitaev model that we have studied and the possible spin liquids observed in α-RuCl$_3$ is currently far from clear, our study highlights the crucial importance of the sign of the Kitaev coupling K in determining the universal properties of these states. While the larger share of studies devoted to determining this sign have advocated that it is ferromagnetic (see, e.g., Refs. [19,20] for summaries), direct experimental inference of this sign has heavily relied on understanding the zigzag AFM state. However, in spite of being an ordered state, the zigzag AFM state is in itself still a highly quantum fluctuating state that delicately depends on perturbations beyond the ideal Kitaev model [3,19,20,24–30]. One alternative state that is comparatively simpler to understand theoretically, but which remains less experimentally explored, is the high-field polarized state. This state could offer a fresh alternative window to perform experiments that could more confidently cement our knowledge of the sign of this important coupling in α-RuCl$_3$.

Note added. Recently, an updated version of Ref. [36] appeared, and our results are in agreement with the various aspects where we overlap with that reference. The updated analysis of Ref. [36] was performed independently and largely in parallel to our work and corrected an earlier version of that reference.

APPENDIX A: VISON HOPPINGS WITH PERIODIC BOUNDARY CONDITIONS

In this Appendix, we present the results of vison hoppings with $(z_1, z_2) = (1, 1)$, i.e., PBCs for ε Majorana fermions. The vison hopping and Berry phases with FM and AFM couplings are shown in Figs. 10 and 12, respectively. At finite κ, the results are essentially the same
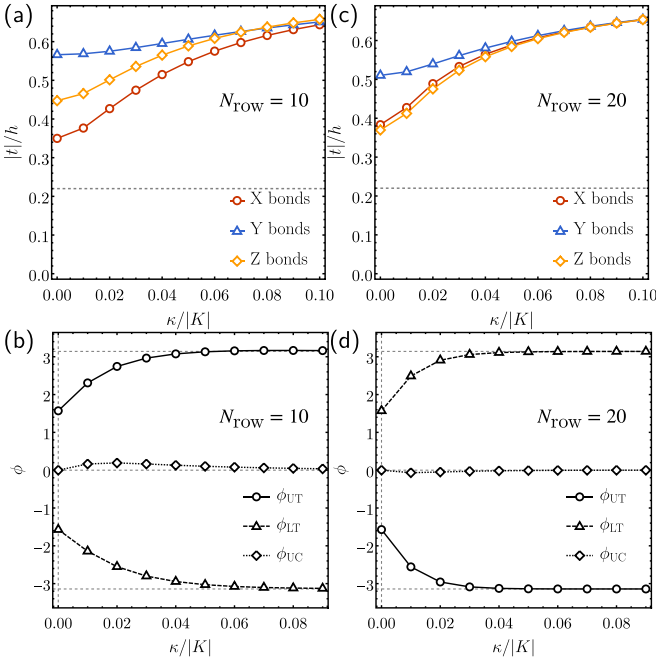
FIG. 11. (a)–(d) The vison hopping amplitude and ϕ with FM coupling at selected system sizes with APBCs for the spinons.

as the APBC results discussed in the main text. For comparison, we also present the APBC results at system size $N_{\text{row}} = 10, \ 20$ with FM (Fig. 11) and AFM Kitaev coupling (Fig. 13).

The Zeeman field is aligned along the [111] direction (the same as in Sec. IV A); we present the results at $\kappa \geqslant 0$, and the Berry phases are obtained with positive h. At finite κ, the vison hoppings and Berry phases are independent of the boundary conditions for both FM and AFM couplings (in the thermodynamic limit). The main difference is at $\kappa = 0$. In the case with APBCs, the results for the system sizes presented here seem to indicate $\phi_{\text{UC}} = 0 \ (\pi)$ for FM (AFM) couplings. On the other hand, with PBCs, the vison hoppings crossing certain bonds could be very small; for example, see the data in Figs. 10(a), 12(a), and 12(c). The smallness of the hopping across certain bonds creates an obstacle to unambiguously identifying the vison hopping phases. For example, as shown in Fig. 12(a), because the vison hopping crossing certain bonds is close to zero, ϕ_{UC} jumps from π to 0 as $\kappa \rightarrow 0$. In Figs. 12(c) and 12(d), although $\phi_{\text{UC}} = \pi$ at $\kappa = 0$, which looks consistent with the APBC result, we caution that such a ϕ_{UC} value is actually extracted from a numerically very small complex number (both the real and imaginary parts being $\sim 10^{-20}$).
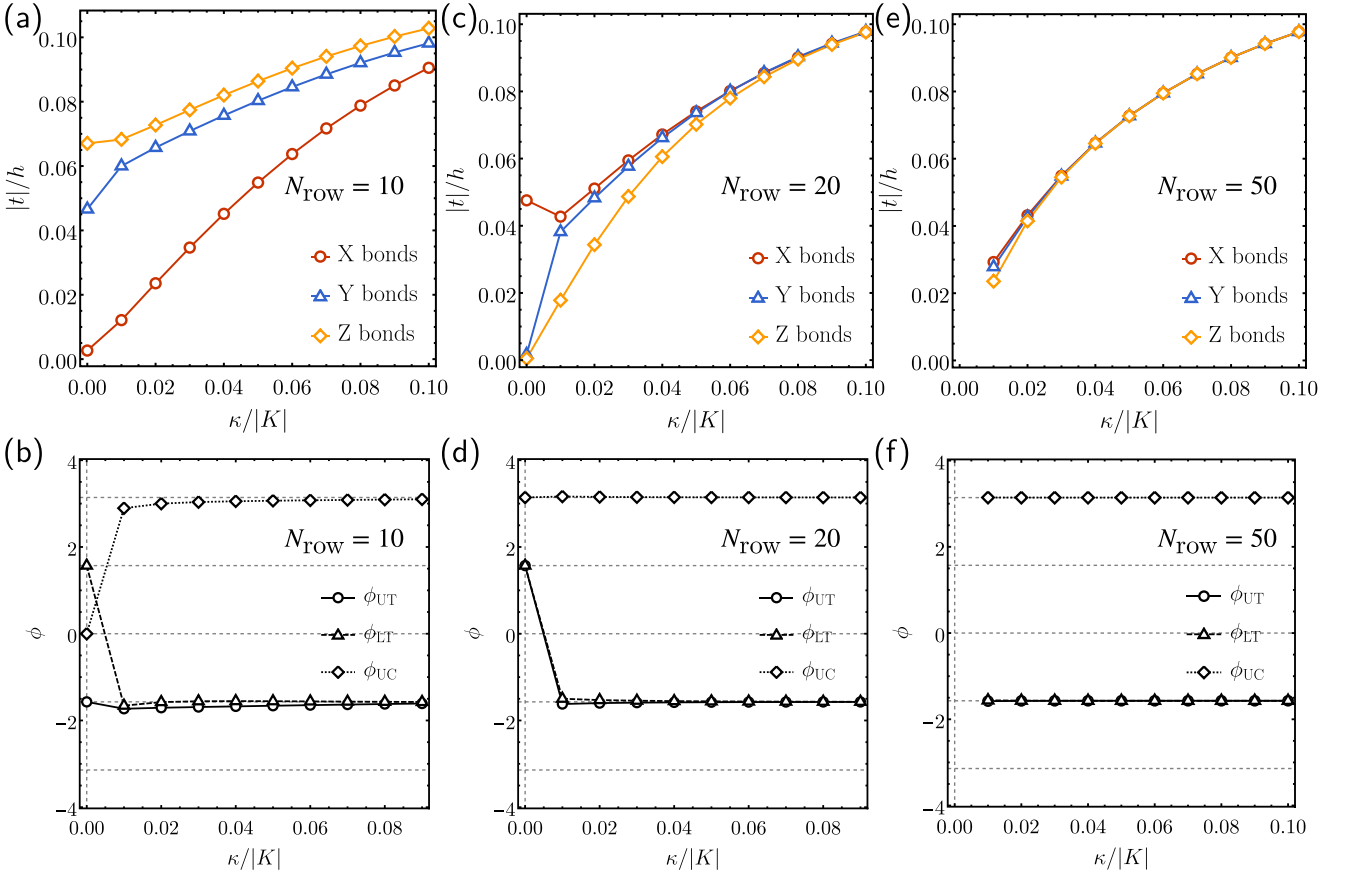

FIG. 12. (a)–(f) The vison hopping amplitude and ϕ with AFM coupling at selected system sizes with PBCs for spinons.
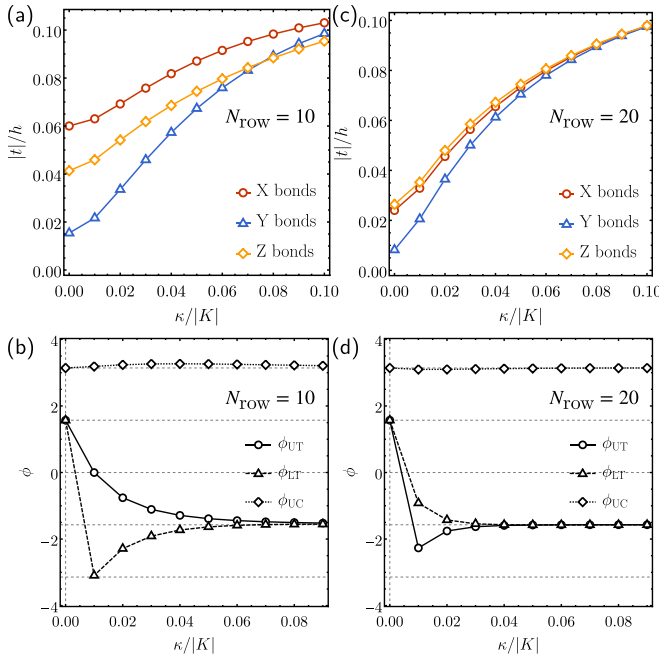
FIG. 13. (a)–(d) The vison hopping amplitude and ϕ with AFM coupling at selected system sizes with APBCs for spinons.

In summary, according to our calculations, while the vison hopping at a finite κ is robust against spinon boundary conditions (Wilson loop sector), the vison hopping at $\kappa = 0$ is very sensitive to the boundary conditions and system sizes. We believe this is due to the gapless nature for the $\kappa = 0$ (B-phase) Kitaev model. Our results then clearly indicate that a small but nonzero κ is needed to properly regularize the vison hopping phases in the fully gapped topologically ordered state.

APPENDIX B: FINITE-SIZE SCALING OF VISON HOPPINGS AND ASSOCIATED PHASES

Within our numerical calculations, the vison hoppings at finite κ converge fast as the system size ($N_{\text{row}} \times N_{\text{row}}$) increases. Results at $\kappa = 0.01|K|$ and $\kappa = 0.02|K|$ with APBCs are presented in Fig. 14. Results with FM coupling are shown in Figs. 14(a) and 14(b), and those with AFM coupling are shown in Figs. 14(c) and 14(d).

It was found that the convergence of vison hoppings with respect to N_{row} is faster at larger κ values. This also gives extra evidence of the strong sensitivity of the vison hoppings to system size in the case of a strictly zero Haldane mass term, $\kappa = 0$.
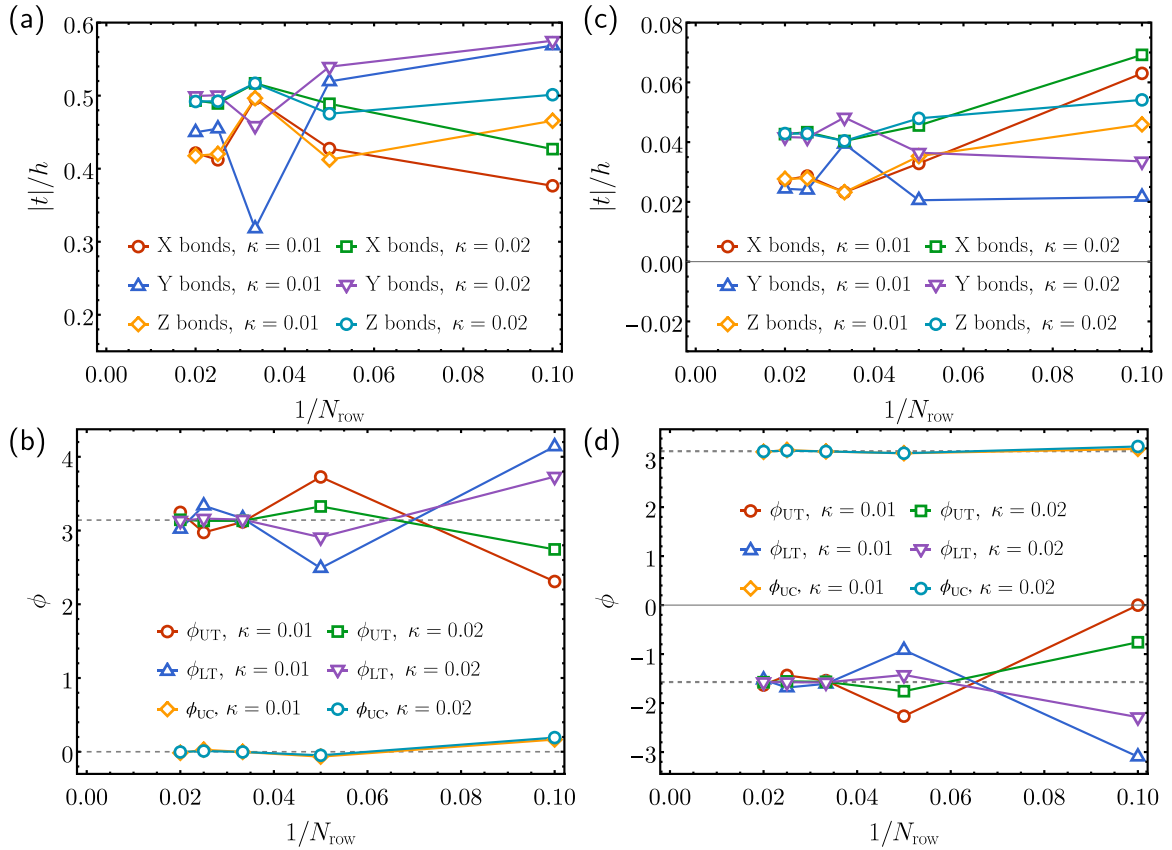

FIG. 14. The scaling of vison hopping amplitudes and ϕ vs $1/N_{\text{row}}$. (a) and (b) Results with $K = -1$. (c) and (d) Results with $K = 1$.

[1] A. Kitaev, Anyons in an exactly solved model and beyond, Ann. Phys. (Amsterdam) **321**, 2 (2006).

[2] G. Jackeli and G. Khaliullin, Mott Insulators in the Strong Spin-Orbit Coupling Limit: From Heisenberg to a Quantum Compass and Kitaev Models, Phys. Rev. Lett. **102**, 017205 (2009).

[3] S. M. Winter, A. A. Tsirlin, M. Daghofer, J. van den Brink, Y. Singh, P. Gegenwart, and R. Valentí, Models and materials for generalized Kitaev magnetism, J. Phys.: Condens. Matter **29**, 493002 (2017).

[4] H. Takagi, T. Takayama, G. Jackeli, G. Khaliullin, and S. E. Nagler, Concept and realization of Kitaev quantum spin liquids, Nat. Rev. Phys. **1**, 264 (2019).

[5] R. D. Johnson, S. C. Williams, A. A. Haghighirad, J. Singleton, V. Zapf, P. Manuel, I. I. Mazin, Y. Li, H. O. Jeschke, R. Valentí, and R. Coldea, Monoclinic crystal structure of $\alpha-$RuCl$_3$ and the zigzag antiferromagnetic ground state, Phys. Rev. B **92**, 235119 (2015).

[6] H. B. Cao, A. Banerjee, J.-Q. Yan, C. A. Bridges, M. D. Lumsden, D. G. Mandrus, D. A. Tennant, B. C. Chakoumakos, and S. E. Nagler, Low-temperature crystal and magnetic structure of $\alpha-$RuCl$_3$, Phys. Rev. B **93**, 134423 (2016).

[7] A. Banerjee, P. Lampen-Kelley, J. Knolle, C. Balz, A. A. Aczel, B. Winn, Y. Liu, D. Pajerowski, J. Yan, C. A. Bridges, A. T. Savici, B. C. Chakoumakos, M. D. Lumsden, D. A. Tennant, R. Moessner, D. G. Mandrus, and S. E. Nagler, Excitations in the field-induced quantum spin liquid state of α-RuCl$_3$, npj Quantum Mater. **3**, 8 (2018).

[8] Y. Kasahara, K. Sugii, T. Ohnishi, M. Shimozawa, M. Yamashita, N. Kurita, H. Tanaka, J. Nasu, Y. Motome, T. Shibauchi, and Y. Matsuda, Unusual Thermal Hall Effect in a Kitaev Spin Liquid Candidate $\alpha-$RuCl$_3$, Phys. Rev. Lett. **120**, 217205 (2018).

[9] A. Banerjee, C. A. Bridges, J.-Q. Yan, A. A. Aczel, L. Li, M. B. Stone, G. E. Granroth, M. D. Lumsden, Y. Yiu, J. Knolle, S. Bhattacharjee, D. L. Kovrizhin, R. Moessner, D. A. Tennant, D. G. Mandrus, and S. E. Nagler, Proximate Kitaev quantum spin liquid behaviour in a honeycomb magnet, Nat. Mater. **15**, 733 (2016).

[10] L. J. Sandilands, Y. Tian, K. W. Plumb, Y.-J. Kim, and K. S. Burch, Scattering Continuum and Possible Fractionalized Excitations in $\alpha-$RuCl$_3$, Phys. Rev. Lett. **114**, 147201 (2015).

[11] J. Nasu, J. Knolle, D. L. Kovrizhin, Y. Motome, and R. Moessner, Fermionic response from fractionalization in an insulating two-dimensional magnet, Nat. Phys. **12**, 912 (2016).

[12] J. Yoshitake, J. Nasu, and Y. Motome, Fractional Spin Fluctuations as a Precursor of Quantum Spin Liquids: Majorana Dynamical Mean-Field Study for the Kitaev Model, Phys. Rev. Lett. **117**, 157203 (2016).

[13] S. Suetsugu, Y. Ukai, M. Shimomura, M. Kamimura, T. Asaba, Y. Kasahara, N. Kurita, H. Tanaka, T. Shibauchi, J. Nasu, Y. Motome, and Y. Matsuda, Evidence for the first-order topological phase transition in a Kitaev spin liquid candidate α-RuCl$_3$, J. Phys. Soc. Jpn. **91**, 124703 (2022).

[14] Y. Kasahara, T. Ohnishi, Y. Mizukami, O. Tanaka, S. Ma, K. Sugii, N. Kurita, H. Tanaka, J. Nasu, Y. Motome, T. Shibauchi, and Y. Matsuda, Majorana quantization and half-integer thermal quantum Hall effect in a Kitaev spin liquid, Nature (London) **559**, 227 (2018).

[15] T. Yokoi, S. Ma, Y. Kasahara, S. Kasahara, T. Shibauchi, N. Kurita, H. Tanaka, J. Nasu, Y. Motome, C. Hickey, S. Trebst, and Y. Matsuda, Half-integer quantized anomalous thermal Hall effect in the Kitaev material candidate α-RuCl$_3$, Science **373**, 568 (2021).

[16] J. A. N. Bruin, R. R. Claus, Y. Matsumoto, N. Kurita, H. Tanaka, and H. Takagi, Robustness of the thermal Hall effect close to half-quantization in α-RuCl$_3$, Nat. Phys. **18**, 401 (2022).

[17] O. Tanaka, Y. Mizukami, R. Harasawa, K. Hashimoto, K. Hwang, N. Kurita, H. Tanaka, S. Fujimoto, Y. Matsuda, E.-G. Moon, and T. Shibauchi, Thermodynamic evidence for a field-angle-dependent Majorana gap in a Kitaev spin liquid, Nat. Phys. **18**, 429 (2022).

[18] P. Czajka, T. Gao, M. Hirschberger, P. Lampen-Kelley, A. Banerjee, J. Yan, D. G. Mandrus, S. E. Nagler, and N. P. Ong, Oscillations of the thermal conductivity in the spin-liquid state of α-RuCl$_3$, Nat. Phys. **17**, 915 (2021).

[19] P. Laurell and S. Okamoto, Dynamical and thermal magnetic properties of the Kitaev spin liquid candidate α-RuCl$_3$, npj Quantum Mater. **5**, 2 (2020).

[20] P. A. Maksimov and A. L. Chernyshev, Rethinking $\alpha-$RuCl$_3$, Phys. Rev. Res. **2**, 033011 (2020).

[21] J. A. Sears, L. E. Chern, S. Kim, P. J. Bereciartua, S. Francoual, Y. B. Kim, and Y.-J. Kim, Ferromagnetic Kitaev interaction and the origin of large magnetic anisotropy in α-RuCl$_3$, Nat. Phys. **16**, 837 (2020).

[22] J. Chaloupka and G. Khaliullin, Magnetic anisotropy in the Kitaev model systems Na$_2$IrO$_3$ and RuCl$_3$, Phys. Rev. B **94**, 064435 (2016).

[23] H. Suzuki, H. Liu, J. Bertinshaw, K. Ueda, H. Kim, S. Laha, D. Weber, Z. Yang, L. Wang, H. Takahashi, K. Fürsich, M. Minola, B. V. Lotsch, B. J. Kim, H. Yavaş, M. Daghofer, J. Chaloupka, G. Khaliullin, H. Gretarsson, and B. Keimer, Proximate ferromagnetic state in the Kitaev model material α-RuCl$_3$, Nat. Commun. **12**, 4512 (2021).

[24] C. Hickey and S. Trebst, Emergence of a field-driven $U(1)$ spin liquid in the Kitaev honeycomb model, Nat. Commun. **10**, 530 (2019).

[25] Z. Zhu, I. Kimchi, D. N. Sheng, and L. Fu, Robust non-Abelian spin liquid and a possible intermediate phase in the antiferromagnetic Kitaev model with magnetic field, Phys. Rev. B **97**, 241110(R) (2018).

[26] J. S. Gordon, A. Catuneanu, E. S. Sørensen, and H.-Y. Kee, Theory of the field-revealed Kitaev spin liquid, Nat. Commun. **10**, 2470 (2019).

[27] M. Gohlke, R. Moessner, and F. Pollmann, Dynamical and topological properties of the Kitaev model in a [111] magnetic field, Phys. Rev. B **98**, 014418 (2018).

[28] J. G. Rau and H.-Y. Kee, Trigonal distortion in the honeycomb iridates: Proximity of zigzag and spiral phases in Na$_2$IrO$_3$, arXiv:1408.4811.

[29] H.-S. Kim, V. S. V., A. Catuneanu, and H.-Y. Kee, Kitaev magnetism in honeycomb RuCl$_3$ with intermediate spin-orbit coupling, Phys. Rev. B **91**, 241110(R) (2015).

[30] E. S. Sørensen, A. Catuneanu, J. S. Gordon, and H.-Y. Kee, Heart of Entanglement: Chiral, Nematic, and Incommensurate Phases in the Kitaev-Gamma Ladder in a Field, Phys. Rev. X **11**, 011013 (2021).

[31] N. Read and B. Chakraborty, Statistics of the excitations of the resonating-valence-bond state, Phys. Rev. B **40**, 7133 (1989).

[32] S. Kivelson, Statistics of holons in the quantum hard-core dimer gas, Phys. Rev. B **39**, 259 (1989).

[33] N. Read and S. Sachdev, Large-*N* Expansion for Frustrated Quantum Antiferromagnets, Phys. Rev. Lett. **66**, 1773 (1991).

[34] T. Senthil and M. P. A. Fisher, Z_2 gauge theory of electron fractionalization in strongly correlated systems, Phys. Rev. B **62**, 7850 (2000).

[35] N. Read and D. Green, Paired states of fermions in two dimensions with breaking of parity and time-reversal symmetries and the fractional quantum Hall effect, Phys. Rev. B **61**, 10267 (2000).

[36] A. P. Joy and A. Rosch, Dynamics of Visons and Thermal Hall Effect in Perturbed Kitaev Models, Phys. Rev. X **12**, 041004 (2022).

[37] C. Chen, P. Rao, and I. Sodemann, Berry phases of vison transport in Z_2 topological ordered states from exact fermion-flux lattice dualities, Phys. Rev. Res. **4**, 043003 (2022).

[38] Y.-A. Chen, A. Kapustin, and Đ. Radičević, Exact bosonization in two spatial dimensions and a new class of lattice gauge theories, Ann. Phys. (Amsterdam) **393**, 234 (2018).

[39] O. Pozo, P. Rao, C. Chen, and I. Sodemann, Anatomy of Z_2 fluxes in anyon Fermi liquids and Bose condensates, Phys. Rev. B **103**, 035145 (2021).

[40] P. Rao and I. Sodemann, Theory of weak symmetry breaking of translations in Z_2 topologically ordered states and its relation to topological superconductivity from an exact lattice Z_2 charge-flux attachment, Phys. Rev. Res. **3**, 023120 (2021).

[41] A. Kapustin and L. Fidkowski, Local commuting projector Hamiltonians and the quantum Hall effect, Commun. Math. Phys. **373**, 763 (2020).

[42] G. Baskaran, S. Mandal, and R. Shankar, Exact Results for Spin Dynamics and Fractionalization in the Kitaev Model, Phys. Rev. Lett. **98**, 247201 (2007).

[43] K. S. Tikhonov, M. V. Feigel'man, and A. Y. Kitaev, Power-Law Spin Correlations in a Perturbed Spin Model on a Honeycomb Lattice, Phys. Rev. Lett. **106**, 067203 (2011).

[44] S. Mandal, S. Bhattacharjee, K. Sengupta, R. Shankar, and G. Baskaran, Confinement-deconfinement transition and spin correlations in a generalized Kitaev model, Phys. Rev. B **84**, 155121 (2011).

[45] J. Knolle, D. L. Kovrizhin, J. T. Chalker, and R. Moessner, Dynamics of fractionalization in quantum spin liquids, Phys. Rev. B **92**, 115127 (2015).

[46] X.-Y. Song, Y.-Z. You, and L. Balents, Low-Energy Spin Dynamics of the Honeycomb Spin Liquid Beyond the Kitaev Limit, Phys. Rev. Lett. **117**, 037209 (2016).

[47] X.-G. Wen, Quantum orders and symmetric spin liquids, Phys. Rev. B **65**, 165113 (2002).

[48] X.-G. Wen, Quantum order: A quantum entanglement of many particles, Phys. Lett. A **300**, 175 (2002).

[49] A. M. Essin and M. Hermele, Classifying fractionalization: Symmetry classification of gapped Z_2 spin liquids in two dimensions, Phys. Rev. B **87**, 104406 (2013).

[50] A. Y. Kitaev, Fault-tolerant quantum computation by anyons, Ann. Phys. (Amsterdam) **303**, 2 (2003).

[51] L. M. Robledo, Sign of the overlap of Hartree-Fock-Bogoliubov wave functions, Phys. Rev. C **79**, 021302(R) (2009).

[52] We only accessed $\kappa = 0$ for $N_{row} \lesssim 20$ due to the slow convergence. This is why this point is missing for $N_{row} = 50$ in Figs. 3(c) and 3(d).

[53] S.-P. Kou and X.-G. Wen, Translation-symmetry-protected topological orders in quantum spin systems, Phys. Rev. B **80**, 224406 (2009).

[54] S.-P. Kou and X.-G. Wen, Translation-invariant topological superconductors on a lattice, Phys. Rev. B **82**, 144501 (2010).

[55] C.-K. Chiu, J. C. Y. Teo, A. P. Schnyder, and S. Ryu, Classification of topological quantum matter with symmetries, Rev. Mod. Phys. **88**, 035005 (2016).

[56] Those states with only two nontrivial $\zeta_k = -1$ and $C = 0$ are "weak topological superconductors," namely, stacks of lower-dimensional superconductors. These states display "weak symmetry breaking" [40], and accordingly, the visons cannot be transported by local operators to all the nearest-neighbor sites of the Bravais lattice.

[57] This state is also labeled as "AI$_0$" in Ref. [40] and is labeled as "A_+" in a recent general classification of the Abelian Z_2 spin liquids (those with $C = 0$) enriched by lattice translations [62].

[58] This state is labeled as "AI$_1$" in Ref. [40] and is labeled as "A^ε" in the recent general classification of the Abelian Z_2 spin liquids enriched by lattice translations of Ref. [62].

[59] We have conjectured in Ref. [37] that states with only one nontrivial parity index have $\phi_{UC} = 0$, whereas states with three nontrivial parity indices have $\phi_{UC} = \pi$. Our current numerics add further evidence to that conjecture.

[60] S.-S. Zhang, G. B. Halász, W. Zhu, and C. D. Batista, Variational study of the Kitaev-Heisenberg-gamma model, Phys. Rev. B **104**, 014411 (2021).

[61] S.-S. Zhang, G. B. Halász, and C. D. Batista, Theory of the Kitaev model in a [111] magnetic field, Nat. Commun. **13**, 399 (2022).

[62] X.-Y. Song and T. Senthil, Translation-enriched Z_2 spin liquids and topological vison bands: Possible application to α-RuCl$_3$, arXiv:2206.14197.